Publications of the Astronomical Society of Australia (PASA), Vol. 33, e001, 7 pages (2016).

doi:10.1017/pasa.2015.52

The XXL Survey XIV. AAOmega Redshifts for the Southern XXL Field

C. Lidman[1,21], F. Ardila[1,2], M. Owers[1,3], C. Adami[4], L. Chiappetti[5], F. Civano[6,7], A. Elyiv[8,9], F. Finet[10,11], S. Fotopoulou[12], A. Goulding[12,13], E. Koulouridis[14], O. Melnyk[15,16], F. Menanteau[17,18], F. Pacaud[19], M. Pierre[14], M. Plionis[20], J. Surdej[11] and T. Sadibekova[14,*]

[1]Australian Astronomical Observatory, North Ryde, NSW 2113, Australia
[2]Department of Astronomy, University of Florida, Gainesville, FL 32611, USA
[3]Department of Physics and Astronomy, Macquarie University, NSW 2109, Australia
[4]LAM, OAMP, Université Aix-Marseille CNRS, Pole de l'Etoile, Site de Château Gombert, 38 rue Frédéric Joliot-Curie, 13388, Marseille 13 Cedex, France
[5]INAF, IASF Milano, via Bassini 15, I-20133 Milano, Italy
[6]Yale Center for Astronomy and Astrophysics, 260 Whitney Avenue, New Haven, CT 06520, USA
[7]Harvard–Smithsonian Center for Astrophysics, 60 Garden Street, Cambridge, MA 02138, USA
[8]Main Astronomical Observatory, Academy of Sciences of Ukraine, 27 Akademika Zabolotnoho St., 03680 Kyiv, Ukraine
[9]Dipartimento di Fisica e Astronomia, Università di Bologna, viale Berti Pichat 6/2, I-40127 Bologna, Italy
[10]Aryabhatta Research Institute of Observational Sciences (ARIES), Manora Peak, Nainital-263 129, Uttarakhand, India
[11]Extragalactic Astrophysics and Space Observations (AEOS), University of Liège, Allée du 6 Août, 17 (Sart Tilman, Bt. B5c), 4000 Liège, Belgium
[12]Department of Astronomy, University of Geneva, ch. d'Ecogia 16, 1290 Versoix, Switzerland
[13]Department of Astrophysical Sciences, Princeton University, Princeton, NJ 08544, USA
[14]Service d'Astrophysique AIM, CEA Saclay, F-91191 Gif sur Yvette, France
[15]Astronomical Observatory, Taras Shevchenko National University of Kyiv, Observatorna str. 3, 04053 Kyiv, Ukraine
[16]Department of Physics, University of Zagreb, Bijenicka cesta 32, HR-10000 Zagreb, Croatia
[17]Department of Astronomy, University of Illinois at Urbana-Champaign, W. Green Street, Urbana, IL 61801, USA
[18]National Center for Supercomputing Applications, University of Illinois at Urbana-Champaign, 1205 W. Clark St., Urbana, IL 61801, USA
[19]Argelander Institut fuer Astronomie, Universität Bonn, D-53121 Bonn, Germany
[20]Aristotle University of Thessaloniki, Department of Physics, Greece
[21]Email: clidman@aao.gov.au

(Received October 05, 2015; Accepted November 28, 2015)

Abstract

We present a catalogue containing the redshifts of 3 660 X-ray selected targets in the XXL southern field. The redshifts were obtained with the AAOmega spectrograph and 2dF fibre positioner on the Anglo-Australian Telescope. The catalogue contains 1 515 broad line AGN, 528 stars, and redshifts for 41 out of the 49 brightest X-ray selected clusters in the XXL southern field.

Keywords: catalogs – surveys – galaxies: clusters: general – galaxies: quasars: general

1 INTRODUCTION

The past decade has seen a dramatic growth in the number of surveys covering large areas of the sky at multiple wavelengths. While these surveys are primarily designed to answer a few key scientific questions, often their greatest value are the data products they provide for use by the broader astronomical community. The XXL survey (http://irfu.cea.fr/xxl) is one such survey.

The XXL survey (Pierre et al. 2015) has used the XMM-Newton X-ray telescope to image 50 deg^2 with a sensitivity of 5×10^{-15} ergs s^{-1} cm^{-2} in the [0.5–2.0] kev band. XXL covers two similarly sized fields that are referred to as the northern XXL field, which is centred on the XMM-LSS survey (Pierre et al. 2004), and the southern XXL field, which is centred in a region covered by the Blanco Cosmology Survey (BCS) (Desai et al. 2012). The XXL survey has detected hundreds of galaxy clusters out to $z \sim 2$ (Pacaud et al. 2015, hereafter, XXL Paper II) and thousands of AGN out to $z \sim 5$ (Fotopoulou et al. 2015).

The key scientific motivation behind the XXL survey, which is described in greater detail in Pierre et al. (2015), is to constrain cosmological parameters using the number density and clustering of X-ray selected clusters. Critical to the success of the survey are a well-characterised proxy

*Data for this paper is deposited here: http://dx.doi.org/10.4225/50/567a71da1efb4.

for cluster masses (Lieu et al. 2015), and redshifts for the clusters.

The northern field has considerably better spectroscopic coverage than the southern field. Within the footprint of the northern field, many tens of thousands of redshifts are publicly available from surveys such as GAMA[1] (Liske et al. 2015) and VIPERS[2] (Guzzo et al. 2014), among others. In comparison, there are many fewer redshifts in the southern XXL field. The XXL collaboration has therefore embarked on a programme of follow-up spectroscopy and imaging on multiple facilities in the Southern Hemisphere, including spectroscopy with the Anglo-Australian Telescope (AAT), imaging with DECam on the CTIO 4m Blanco Telescope (Gardner et al. in preparation) , and radio observations with the Australia Telescope Compact Array (Smolčić et al. 2015).

In this paper, we publish the redshifts that were obtained during three observing runs with the AAT. Around 3 600 redshifts were obtained. The objects targeted broadly consist of three types: Active Galactic Nuclei (AGN), which make up most of the objects, galaxies, and stars.

The paper is structured as follows. In Section 2, we define how targets were selected, summarise the observations, and provide a detailed description of how the data were processed. In the Section 3, we describe the redshift catalogue, and present a few graphs illustrating the key statistics of the survey. Before concluding, we compute the velocity dispersion for those clusters that have at least 10 spectroscopically confirmed members. We then end with a summary of the key aspects of the paper. Throughout our analysis, we adopt the AB magnitude system and the WMAP9 cosmology (Hinshaw et al. 2013) of $H_0 = 70\,\mathrm{km\,s^{-1}Mpc^{-1}}$, $\Omega_M = 0.28$ and $\Omega_\Lambda = 0.72$.

2 TARGET SELECTION, OBSERVATIONS, AND DATA PROCESSING

Targets were selected according to criteria that were designed to select two kinds of objects. The first set of criteria were designed to select AGN, while the second set were designed to select galaxies in clusters and groups.

2.1. AGN

The AGN sample consists of about 4 500 X-ray point-like sources that were within 6 arcsec of an optical source ($16 < r < 22$ mag) from the BCS (Desai et al. 2012). We only considered one counterpart for each X-ray source following the procedure described in Chiappetti et al. (2013) and Melnyk et al. (2013). The best ranked counterpart had the highest probability $P_{XO} = \exp(-n(< r)d^2)$ of being associated with the X-ray source (Downes et al. 1986), where d represents the angular distance between the X-ray source and its counterpart, and $n(< r)$ is the density of objects brighter than the r-band magnitude of the considered optical counterpart. The median value of $P_{\rm XO}$ for our sample is 0.9969, with quartiles of 0.9907 and 0.9993. According to Tajer et al. (2007) and Garcet et al. (2007), counterparts with $P_{\rm XO} > 0.99$ are considered good and counterparts with $0.99 > P_{\rm XO} > 0.97$ are considered fair. We did not apply a lower bound to $P_{\rm XO}$, but we did visually inspect all counterparts using the g, r, and i images from the BCS. We deleted from the list all bright stars, artefacts, and objects that were fainter than our $r = 22$ mag cut, which is roughly the limit one can obtain redshifts in a few hours of exposure time on the AAT.

Compared to cluster galaxies, AGN were assigned a lower priority for observation. Hence, there is a bias against observing AGN near clusters. This bias needs to be taken into account when computing the clustering of AGN.

Table 1. Observing dates.

July 05 to July 10	six half nights
September 08 to September 09	two full nights
September 29	one full night

2.2. Cluster galaxies

For the cluster sample, we first selected all objects brighter than $r = 22$ within a 500 kpc radius of the cluster centres. The angles on the sky were derived from the photometric redshifts of the clusters.[3] We then selected objects that satisfy one of two conditions: (i) they have a photometric redshift that differs from the cluster redshift by 0.05 or less (0.05 is the median uncertainty in our photometric redshifts), or (ii) they have a colour that places them within the cluster red sequence. We also manually inserted targets that were of special interest, e.g. a bright galaxy that was not inside the selected ranges listed above, but was likely to be a cluster member.

2.3. Observations

We used the two-degree field (2dF) fibre positioner (Lewis et al. 2002) on the AAT in conjunction with the AAOmega spectrograph (Smith et al. 2004) to observe 4 884 targets in the XXL-South footprint during three observing runs in 2013. The dates of the observing runs are listed in Table 1.

The 2dF fibre positioner can place up to 400 fibres within a 2.1° diameter field-of-view, with the restriction that any two fibres cannot be placed within 30 arcsec to 40 arcsec of each other. Eight fibres are used for guiding, and following the recommendation in the AAOmega User's Manual,[4] 25 fibres were placed in areas free of objects as a means of obtaining a spectrum of the night sky. This leaves of the order of 360 fibres that can then be positioned on objects of interest. The fibre diameter on sky is approximately 2 arcsec.

[1] http://www.gama-survey.org
[2] http://vipers.inaf.it

[3] The photometric redshifts of the clusters span a large range, from $z = 0.1$ to $z = 1$. Over this range of redshifts, angles vary from 60 arcsec at high redshift to 270 arcsec at low redshift.
[4] http://www.aao.gov.au/science/instruments/AAOmega

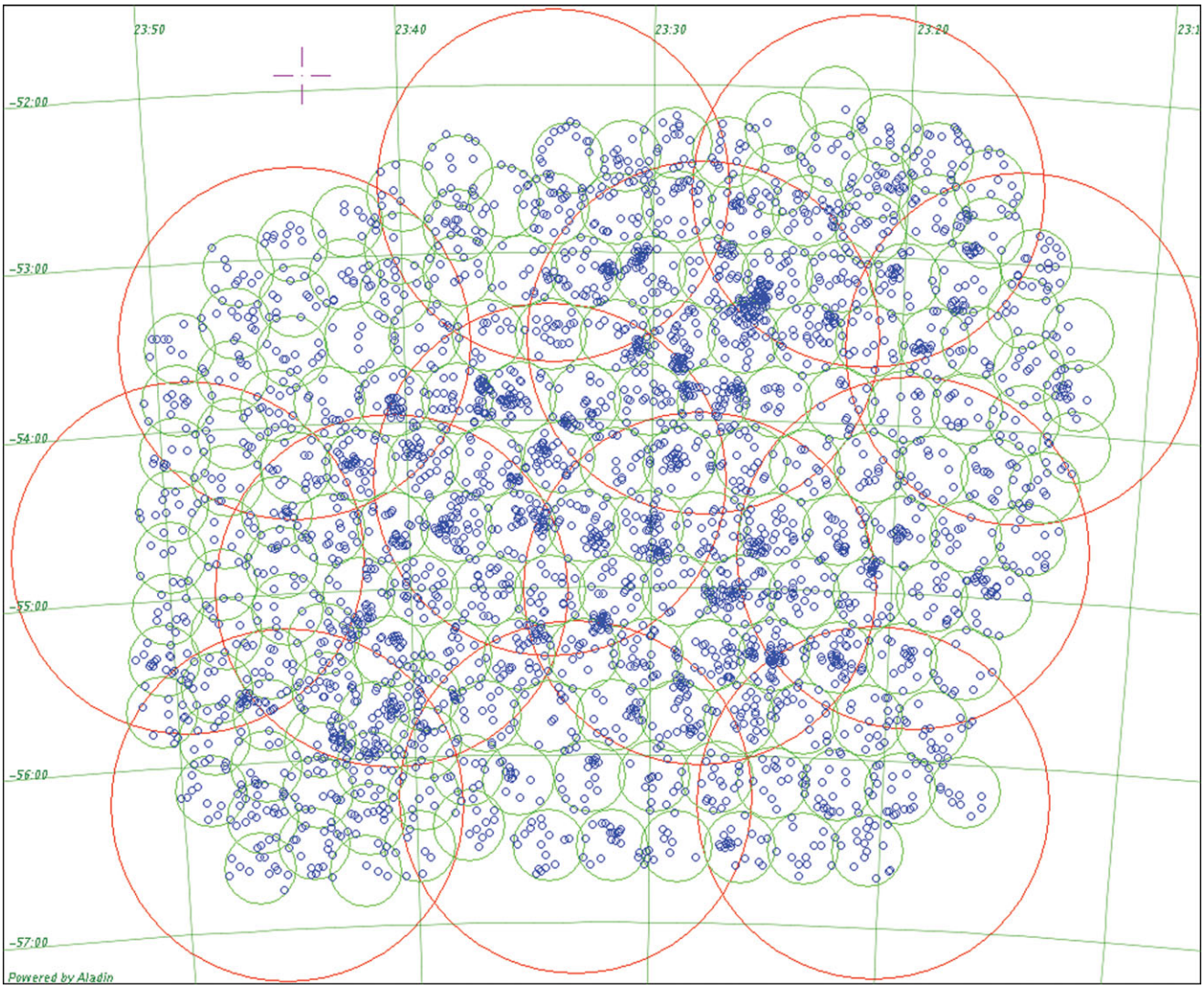

Figure 1. A view of the objects (small blue circles) in the XXL southern field with spectroscopic redshifts from this work. The individual XMM pointings are shown as the green circles. The 13 larger red circles, each 2.1° in diameter (the field of view of 2dF), cover the entire area observed with XMM. Individual clusters can be picked out from the concentration of blue circles in certain areas. This plot was produced with Aladin.

The 2dF fibre positioner can feed either HERMES (Sheinis et al. 2015), a moderate resolution, 4-channel spectrograph, or the AAOmega spectrograph (Smith et al. 2004), which was the instrument used in this study. A dichroic in AAOmega is used to split the light into the red and blue channels of the spectrograph. We used one of the standard setups for our observations: the X5700 dichroic, the 385 R grating in the red channel and the 580 V grating in the blue channel. This results in spectra that start and end at 370 and 890 nm, respectively, with a spectral resolution of about 1 500. The amount of overlap between the two channels varies with fibre number, and is typically 3 nm.

The entire footprint of XXL-South is covered by 13 2dF fields. The field centres of these 13 fields are shown in Figure 1. On average, three hours was spent on each field over the course of the three observing runs.

When configuring each field, highest priority was given to candidate cluster galaxies. Next, highest priority were AGN, followed by sky fibres. Science exposures lasted 30 min, and depending on observing conditions, up to four of these were taken consecutively in an observing sequence. Prior to each sequence, an arc frame and a fibre flat were taken. The arc frame is used to calibrate the wavelength scale of the spectra and the fibre flats are used to determine the locations of the spectra on the charge-coupled device (CCD) (the so-called tramline map), to remove the relative wavelength dependent transmission of the fibres (absolute normalisation is done using night sky lines), and to determine the fibre profile for later use in extracting the spectra from the science frames.

Bias frames and dark frames were taken daily. While these frames are not required for processing data from the CCD in red arm of AAOmega, they are essential for

removing artefacts from data taken with the CCD in the blue arm.

2.4. Data processing

After each run, we processed the raw data with version 5.35 of the `2dfdr` pipeline[5]. Redshifts were then measured (see Section 3), and all objects with secure redshifts were removed from the target catalogue before the next run. This maximised the observing efficiency in the second and third observing runs. After the first run, we also modified the pointings shown in Figure 1 to improve the targeting efficiency.

We have since reprocessed the data with a modified version 6.2 of the `2dfdr` pipeline. Version 6.2 improves on version 5.35 in several notable ways. Tram line mapping is more precise, and one can now simultaneously fit a model of the background scattered light together with the flux in the fibres to each column of the detector. The fibre traces are almost parallel to the detector rows.

The further modifications we made to v6.2 of `2dfdr` improve on the publicly available version is several key aspects. These improvements include:

- Using PyCosmic (Husemann et al. 2012) to find pixels affected by cosmic rays. These pixels are removed from the analysis.
- Using singular value decomposition (SVD) when the least-squares solution fails to produce an adequate solution to the matrix equation that is used to optimally extract the flux in the fibres (see Sharp & Brichall (2010) for details). On average, we use SVD instead of least squares once every 200 columns.
- For low signal-to-noise regions in the fibre flats (typically in the very blue end of the spectrum), average over 10 columns when fitting the fibre profile.
- Using the `2dfdr` provided 2d background subtraction routine instead of the 1d sky subtraction routine to remove the scattered light background before fitting the fibre profiles.

These modifications will be incorporated in future versions of `2dfdr`.

Once processed, we then splice the red and blue ends of the spectra. Since some targets are observed over different nights and can appear in more than one field (because of field overlap) we sum all the data on a single target into one spectrum, weighting on the signal-to-noise ratio.

These improvements lead to better quality data. As a result, we get about 10% more redshifts than we did with version 5.35 of `2dfdr`. While the data are better, there is still room for improvement. In particular, one can sometimes see a discontinuity in the spectra near to wavelength where the dichroic splits the light into the two arms of the spectrograph. This is largely due to errors in sky subtraction and is caused by a combination of residual background scattered light, errors in estimating the normalisation of the fibre throughputs, and poor spectral and spatial uniformity in the fibre flats. The accuracy of the sky subtraction, which is assessed by examining how well the sky is removed from the sky fibres, is about 1% in the continuum.

[5] http://www.aao.gov.au/science/instruments/AAOmega/reduction

3 REDSHIFT ESTIMATES

We used `runz` (Drinkwater et al. 2010) to inspect each spectrum, to measure a redshift, and to note down any relevant aspects, such as the presence of broad emission lines. For each spectrum, we assign a quality flag that varies from 1 to 6. The flags are identical to those used in the OzDES redshift survey (Fang et al. 2015), and have the following meanings:

- 6 - a star
- 4 - $>$ 99% redshift consistency in overlap regions
- 3 - $\sim$ 95% redshift consistency in overlap regions
- 2 - an educated guess
- 1 - unknown

Only objects with flag 3, 4, and 6 are listed in our catalogue. Flag 5 is an internal flag used by OzDES, and is not used here. The fraction of objects with the flag set to 6, 4, or 3, or less than 3 were 0.10, 0.53, 0.12, and 0.25, respectively.

All redshifts are placed in the heliocentric reference frame. The correction is small, usually less than 0.0001 in redshift. The redshift completeness as a function of magnitude and the redshift quality flag is shown in Figure 2 for AGN and cluster galaxies.

3.1. Redshift uncertainties

The considerable overlap between fields (see Figure 1) means that about 700 objects were observed more than once. We noted earlier that we had processed the data twice, once with an earlier version of 2dfdr and again with a revised version. On the first occasion, we measured redshifts of objects in each field independently. By comparing the redshifts of objects in the overlap regions, we get an estimate of redshift uncertainties and an estimate of the number of times the redshifts agree.

For objects with the flag set to 4 or 6, there were no inconsistent redshifts. For objects that have the flag set to 3, the percentage of objects with consistent redshifts was 95%.

We use these repeat observations to also measure the RMS difference between pairs of observations. We estimate the redshift uncertainty by dividing the RMS by $\sqrt{2}$. The uncertainty depends on object type. For AGN, which generally have broad lines, the uncertainty is typically $0.001(1+z)$. For galaxies, the corresponding uncertainty is $0.0002(1+z)$.

Table 2. The first four objects in the redshift catalogue.

Name	R.A. (J2000) (deg)	Dec. (J2000) (deg)	Redshift	Redshift flag	Comment
XXL-AAOmega J234817.22-541456.6	357.07175	−54.24905	2.2079	4	AGN
XXL-AAOmega J234853.07-534134.0	357.22113	−53.69278	0.6792	4	AGN
XXL-AAOmega J234926.54-534618.2	357.36060	−53.77172	1.6434	4	AGN
XXL-AAOmega J234937.79-534724.9	357.40747	−53.79025	0.2560	4	AGN

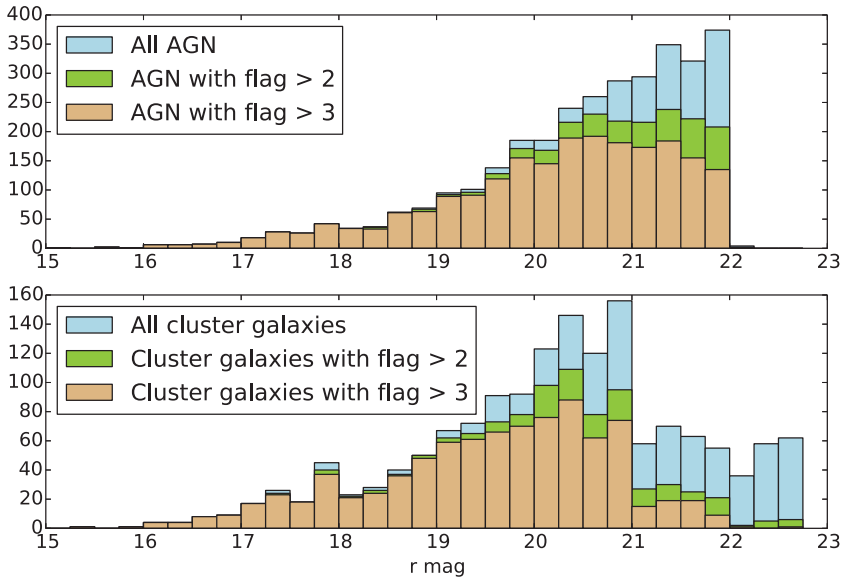

Figure 2. Redshift completeness as a function of *r*-band magnitude for AGN (above) and cluster galaxies (below).

3.2. The redshift catalogue and object demographics

The first four lines of the catalogue are shown in Table 2. The full catalogue can be obtained from CESAM[6], via the XXL Master Catalogue Browser[7], or by contacting the first author of this paper.

The comment field is usually blank or has one of two values: AGN or binary. If broad AGN-like features are visible in the spectrum, then we mark the object as an AGN (see Figure 3 for an example of an object with broad emission lines). About half of the 3 184 targeted X-ray point sources have broad AGN-like features. Redshifts for about half of the sources that remain (i.e. those without broad lines) could be obtained from galaxy lines. The remaining sources, about 25% of the total, do not have a redshift. About 7% of the X-ray point sources were stars (the redshift quality flag is set to 6 for such objects). A detailed breakdown of the number of redshifts obtained is provided in Table 3.

The comment 'binary' means that the spectral features of two stars, usually an M dwarf with a white dwarf, are visible in the spectrum. There are three of these in the catalogue.

Table 3. The number of objects targeted and the number of redshifts obtained.

Object	Objects targeted	Objects with redshifts (excludes stars)	Stars	Objects with broad AGN-like features
AGN	3 184	2 332	220	1,533
Cluster galaxies	1 674	830	278	26
Total	4 858	3 162	498	1,559

Of the 1 674 objects targeted as candidate cluster galaxies, 830 have redshifts. Broad AGN-like features could be seen in 26 of the spectra. Another 278 objects are stars, of which nearly all are M dwarfs.

In Figure 1, we show the distribution of objects with redshifts on the sky, and in Figure 4, we show the redshift distribution of AGN, and galaxies. Galaxies are largely restricted to be below $z \sim 1$, whereas AGN go out to $z \sim 5$.

Also shown in Figure 4 is the redshift distribution (scaled by x5) of 41 galaxy clusters whose redshifts were measured through these observations. These 41 clusters represent a subsample of the 100 most X-ray luminous clusters (49 of

[6] http://cesam.oamp.fr/xmm-lss/
[7] http://cosmosdb.iasf-milano.inaf.it/XXL

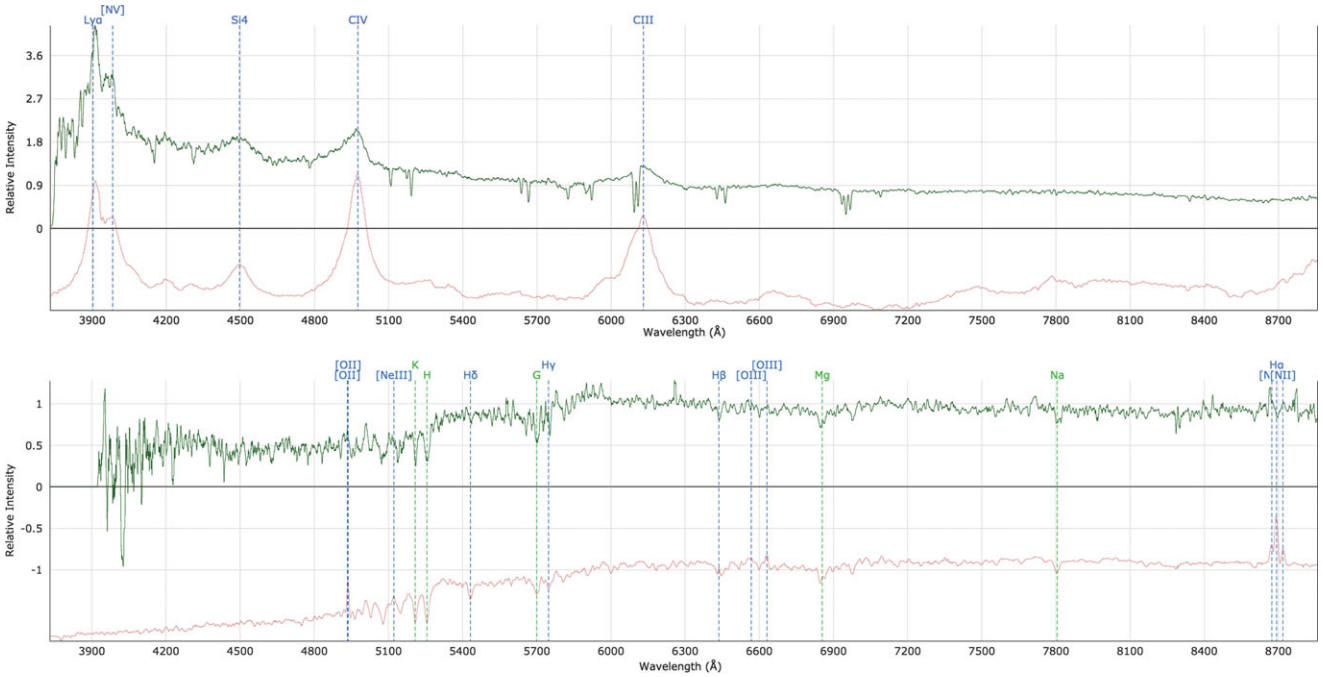

Figure 3. Sample spectra (in green) showing an AGN with broad emission lines (above) and a cluster galaxy (below). Template spectra are shown in red. The vertical lines mark commonly observed lines in AGN and galaxies. This plot was produced using the output from `Marz` (Hinton et al. in preparation).

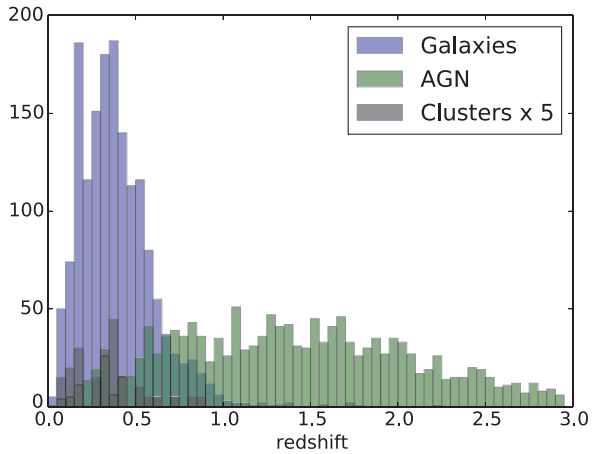

Figure 4. A redshift histogram of AGN, clusters (scaled by x5) and galaxies in the XXL southern field. The AGN extend out to $z \sim 5$, and the clusters out to $z \sim 0.9$. Not shown are the 44 AGN in the redshift interval $3 \leq z \leq 5$.

which are in XXL-South[8]) listed in XXL Paper II. For this subsample, we targeted 838 objects within 1 Mpc of the cluster X-ray centres. Of these, we obtained redshifts for 501 galaxies, of which 211 were found to belong to the cluster.

4 VELOCITY DISPERSIONS

The nearest clusters have the largest angular extent on the sky, so it was sometimes possible to allocate more than one fibre to cluster members in a single plate configuration. Sometimes this was as high as five. We were also able to free up fibres in later runs once a redshift was obtained, and there is quite some overlap between the 13 AAOmega pointings. Altogether, this meant that some of the nearer clusters have over a dozen spectroscopically confirmed members from the AAOmega spectroscopy alone. This is sufficient to measure a velocity dispersion.

Using the location of the 49 brightest X-ray selected clusters listed in XXL Paper II, we select galaxies as potential cluster members if they satisfy the following criteria. They have more than 10 members with redshifts that land within $0.01 * (1 + z_{cl})$ of the cluster redshift z_{cl} and have positions that land within 1 Mpc of the cluster centre. There are eight such clusters in total. From these members, we use either the biweight midvariance or the gapper (Beer, Flynn, & Gebhardt 1990) as a robust estimator of the velocity dispersion. The former is used if there are more than 15 objects; while the latter is used otherwise. For our sample, there is little difference between the two methods. The results are listed in Table 4. The uncertainties of both methods are estimated using bootstrap resampling. The uncertainties in the redshifts translate to an uncertainty of $\sim$80 km s^{-1} at $z \sim 0.3$. The impact of these uncertainties on the velocity dispersions that are computed for these clusters is negligible.

The X-ray centroids of XLSSC 535 and XLSSC 536, which are the X-ray counterparts of Abell 4005, are separated by 3.5 arcmin, which corresponds to 600 kpc at $z = 0.17$. The 24 spectroscopic members observed do not show evidence of a bimodal distribution in redshift. Hence,

[8]The redshifts of the remaining eight clusters have been or are currently being obtained with other facilities. See XXL Paper II for details.

Table 4. Cluster velocity dispersions for 8 of the 49 clusters in XXL Paper II.

Cluster	z	Members	Vel. disp. [km/s]
XLSSC 535/536[a]	0.171	24	660^{+90}_{-110}
XLSSC 524[b]	0.270	11	640^{+100}_{-200}
XLSSC 538	0.332	13	1080^{+170}_{-320}
XLSC 544	0.095	11	530^{+100}_{-200}
XLSSC 545	0.353	12	370^{+20}_{-80}
XLSSC 547	0.367	16	810^{+100}_{-160}
XLSSC 548	0.321	14	800^{+60}_{-180}

[a]The X-ray counterpart to Abell 4005
[b]Cluster 511 in Šuhada et al. (2012)

we consider them together, when measuring the velocity dispersion.

There is a positive correlation between the velocity dispersions listed in Table 4 and the X-ray determined masses that are listed in XXL Paper II; however, given the size of the sample (only eight clusters) and the large uncertainties in both the mass and the velocity dispersion, the correlation is not significant.

5 SUMMARY

Using AAOmega on the AAT, we have obtained the redshifts of 3 660 X-ray selected sources in the XXL southern field. Of these 3 660 sources, 1 558 are broad line AGN, and 498 are stars. The remaining objects are either galaxies from the AGN sample without broad lines, field galaxies, or cluster galaxies in XXL detected clusters.

Of the 49 brightest X-ray selected clusters in the XXL southern field, we get redshifts for 41 of them. We compute the velocity dispersions for clusters with more than 10 members. The velocity dispersions are indicative of clusters that range from rich groups to massive clusters.

ACKNOWLEDGEMENTS

Based in part on data acquired through the Australian Astronomical Observatory, under programmes A/2013A/018 and A/2013B/001. O.M. is grateful for the financial support provided by the NEWFELPRO fellowship project in Croatia. F.P. acknowledges support from the BMBF/DLR grant 50 OR 1117, the DFG grant RE 1462-6 and the DFG Transregio Programme TR33.

REFERENCES

Beer, B. C., Flynn, K., & Gebhardt, K. 1990, AJ, 100, 32
Chiappetti, L., et al. 2013, MNRAS, 429, 1652
Desai, S., et al. 2012, ApJ, 757, 83
Downes, A. J. B., Peacock, J. A., Savage, A., & Carrie, D. R. 1986, MNRAS, 218, 31
Drinkwater, M. J., et al. 2010, MNRAS, 401, 1429
Fang, Y., et al. 2015, MNRAS, 452, 3047
Garcet, O., et al. 2007, A&A, 474, 473
Guzzo, L., et al. 2014, A&A, 566, 108
Hinshaw, G., et al. 2013, ApJS, 208, 19
Husemann, B., et al. 2012, A&A, 545, 137
Lewis, I., et al. 2002, MNRAS, 333, 279
Liske, J., et al. 2015, MNRAS, 452, 2087
Melnyk, O., et al. 2013, A&A, 557, 81
Pierre, M., et al. 2004, JCAP, 9, 11
Sheinis, A., et al. 2015, JATIS, 1, 035002
Šuhada, R., et al. 2012, A&A, 537, A39
Sharp, R., & Brichall, M. 2010, PASA, 27, 91
Smith, G. A., et al. 2004, in SPIE Conf. Ser., Vol. 5492, Ground-based Instrumentation for Astronomy, ed. A. F. M. Moorwood & M. Iye (Bellingham: SPIE), 410
Tajer, M., et al. 2007, A&A, 467, 73
XXL Paper I: Pierre, M., et al. 2015, A&A, in press, arXiv:1512.04317
XXL Paper II: Pacaud, F., et al. 2015, A&A, in press, arXiv:1512.04264
XXL Paper IV: Lieu, M., et al. 2015, A&A, in press, arXiv:1512.03857
XXL Paper VI: Fotopoulou, S., et al. 2015, A&A, submitted
XXL Paper XI: Smolčić, V., et al. 2015, A&A, in press, arXiv:1512.04322